Slow Magnetic Relaxation in Dinuclear CoY Complexes

Joydev Acharya, Abinash Swain, Amit Chakraborty, Vierandra Kumar, Pawan Kumar, Jessica Flores Gonzalez, Olivier Cador, Fabrice Pointillart, Gopalan Rajaraman, Vadapalli Chandrasekhar

Slow Magnetic Relaxation in Dinuclear $Co^{II}Y^{III}$ Complexes

Joydev Acharya,[a] *Abinash Swain,* [b]*Amit Chakraborty,*[a,d] *Vierandra Kumar,*[a] *Pawan Kumar,*[a] *Jessica Flores Gonzalez,*[c] *Olivier Cador,*[c] *Fabrice Pointillart,**[c] *Gopalan Rajaraman,**[b] *and Vadapalli Chandrasekhar**[a,d]

[a]Department of Chemistry, Indian Institute of Technology Kanpur, Kanpur-208016, India.

E-mail: vc@iitk.ac.in

[b]Department of Chemistry, Indian Institute of Technology Bombay, Powai,Mumbai-400 076, India. E-mail: rajaraman@chem.iitb.ac.in

[c]Institut des Sciences Chimiques de Rennes, UMR 6226 CNRS-Université deRennes 1,263 Avenue du Général Leclerc, 35042 Rennes Cedex, France. E-mail: fabrice.pointillart@univ-rennes1.fr

[d]Tata Institute of Fundamental Research, 36/P, Gopanpally Village, Serilingampally Mandal, Ranga Reddy District, Hyderabad 500107, India.

Abstract

Four new dinuclear complexes, [Co(μ-L)(μ-CCl_3COO)Y$(NO_3)_2$]·2$CHCl_3$·CH_3CN·2H_2O **(1)**, [Co(μ-L)(μ-CH_3COO)Y$(NO_3)_2$]·CH_3CN **(2)**, [Co(μ-L)(μ-PhCOO)Y$(NO_3)_2$]·3CH_3CN·2H_2O **(3)** and [Co(μ-L)(μ-^{t}BuCOO)Y$(NO_3)_2$]·$CHCl_3$·2H_2O **(4)** having a $Co^{II}Y^{III}$ core have been synthesized by employing a ferrocene based compartmental ligand. In all the complexes the main structural motif is kept similar by only slightly varying the substitution on the bridging acetate groups. This variation has resulted a small but subtle influence on the magnetic relaxation of all these four compounds. *Ab initio* CASSCF/NEVPT2 calculations were carried out to assess the effect of the different substitutions of the bridging ligands on the magnetic anisotropy parameters and on orbital arrangements. *Ab initio* calculations yield very large positive D value which is consistent with the geometry around the Co(II) ion and easy plane anisotropy ($g_{xx}>g_{zz}$) with the order of the calculated D in the range of 72.4 to 91.7 cm^{-1} is estimated in this set of complexes. To ascertain the sign of zero-field splitting in these complexes, EPR spectra was recorded which support the sign of D values estimated from *ab initio* calculations.

Introduction

Single-molecule magnets (SMMs), single-ion magnets (SIMs) and single-chain magnets (SCMs) are families of molecular magnets that seem to have considerable promise as materials of the future in applications as diverse as data storage to quantum computing[1]. While it is true that realization of even some of these applications can only be attempted after major challenges in this field are overcome, research in this area continues to grow unabated, driven by an academic interest. One of the qualitative understandings that has emerged as a result of investigations over the last two decades is that in order for a molecule to exhibit the phenomenon of SMM behavior it should possess a large ground state spin and a large magnetic anisotropy such that a bistable ground state, with an energy barrier equal to $|D|S^2$ for integral spin values and $|D|S^2$-1/4 for non-integer spins values, can result (S is total spin and D, a second-order axial anisotropy parameter having value < 0). The negative sign of D is an important parameter for assembling good SMMs because it favors high $|m_s|$ states as the ground state. Thus, several complexes have been reported where the value of axial zero field splitting parameter was negative (D < 0) and found to be good SMMs with slow magnetic relaxation.[2] In contrast when D > 0, the ground state will be the $|m_s| = 0$ for systems with integer S and the $|m_s| = \pm 1/2$ Kramer's doublet for those with non-integer S. In this case it seems that a system with D > 0 should have no energy barrier for spin reversal, as the spin is free to rotate within its easy plane. Interestingly, slow magnetic relaxation has also been observed in systems with an easy plane anisotropy (D > 0).[3] This fact can be explained by the presence of the rhombic zero-field splitting *i.e.* in plane anisotropy given by a $E(S_x^2-S_y^2)$ term where E is second-order rhombic anisotropy parameter and whose value is limited to $0 < E/|D| < 0.33$. For high positive D values the ground state is well separated from the excited state manifolds of the spin multiplets that are not thermally accessible. In such cases the direct relaxation process and two-phonon Raman process becomes significant over Orbach process of the magnetic relaxation.

In 2014 Ruiz and colleagues reported an extensive theoretical study on a model complex of Co^{II}, $[Co(acac)_2(H_2O)_2]$ (acac = acetylacetonate) having D > 0 and stated that slow relaxation of magnetization naturally occurs following the Kramer's theorem, irrespective of the sign of D.[4] Co^{II} being a Kramers ion (S=3/2) is thus a good choice for assembling complexes that can be potential SMMs. We reported the first example of a Co^{II}-Ln^{III} based SMM, $[LCo^{II}$-Gd^{III}-$Co^{II}L]^+$, (LH_3 = (S)P[N(Me)N=CH-C_6H_3-2-OH-3-OCH_3]$_3$, a cationic trinuclear complex several years ago.[5] This was followed by other examples of Co^{II}-Ln^{III} based SMMs.[4, 6] A couple of examples of Co^{II}-Y^{III} complexes where Co^{II} is the only paramagnetic center, with a diamagnetic Y^{III} metal ion as the neighbor, have been reported to act as single ion magnets (SIM).[7] The oxygen bridged diamagnetic metal center not only increases the electron density on the bridged oxygen atom and thereby influencing the electronic environment around the paramagnetic metal center but also provides a diamagnetic surrounding that may help to prevent the intermolecular spin-spin interaction increasing the efficiency of single ion magnet behavior. This hypothesis has been tested in some 3d/4f complexes where the 3d metal ion is diamagnetic.[8] On other hand examples of 3d/4f complexes where the 3d metal ion is paramagnetic and the adjoining metal ion is diamagnetic are still sparse. There are a few Co^{III}-Co^{II} complexes where this phenomenon has been realized.[9]

Recently we have designed a ferrocene-supported ligand, LH_2, {LH_2 = Fe[(C_5H_4){-C(Me)=N-N= CH-C_6H_3-2-OH-3-OCH_3}]$_2$}, that allowed us to assemble dinuclear 3d/4f complexes.[10] We were interested in examining if this ligand would be amenable to construct Co(II)/Y(III) complexes. Accordingly, four complexes $[Co(\mu\text{-L})(\mu\text{-RCOO})Y(NO_3)_2]$ (Scheme 1) were prepared where a bridging carboxylate group between the Co(II) and the Y(III) center is systematically varied [$RCOO^-$ = CCl_3COO^- for **1;** CH_3COO^- for **2**; $PhCOO^-$ for **3**, $^tBuCOO^-$ for **4** respectively]. In the following we report the synthesis, structure, magnetism and theoretical studies on these complexes.

Experimental Section

All the solvents were purified by adopting standard procedures.[11] Acetyl chloride (Spectrochem, Mumbai), ferrocene (Sigma-Aldrich, USA), aluminum chloride, hydrazine hydrate (Spectrochem, Mumbai, India), *o*-vanillin, pivalic acid, benzoic acid, trichloroacetic acid (S.D. Fine Chemicals, Mumbai, India), $Co(OAc)_2 \cdot 4H_2O$, $Y(NO_3)_3 \cdot xH_2O$ and $Co(ClO_4)_2 \cdot 6H_2O$ (Sigma-Aldrich, USA) were used as purchased. Diacetylferrocene and 1,1′-diacetylferrocene dihydrazone were synthesized and purified according to reported procedures.[10]

Instrumentation

Melting points were measured using a JSGW melting point apparatus and are uncorrected. IR spectra were recorded as KBr pellets on a Bruker Vector 22 FT IR spectrophotometer operating at 400–4000 cm^{-1}. ^1H NMR spectra were recorded on a JEOL JNM LAMBDA 400 model spectrometer operating at 500 MHz. Chemical shifts are reported in parts per million (ppm) and are referenced with respect to internal tetramethylsilane (^1H). Elemental analyses of the compounds were obtained from Thermoquest CE instruments CHNS-O, EA/110 model. Electrospray ionization mass spectrometry (ESI-MS) spectra were recorded on a Micromass Quattro II triple quadrupole mass spectrometer. Methanol was used as the solvent for the electrospray ionization (positive ion, full scan mode). Capillary voltage was maintained at 2 kV, and cone voltage was kept at 31 kV. Variable-temperature EPR spectra of compounds 2-4 in powdered were recorded at 5K and 10K using a Bruker spectrometer operating at Q-band (35 GHz) frequency, and the EPR simulation was performed with Easyspin software (version 5.0.0). The dc magnetic susceptibility measurements were performed on solid polycrystalline samples (the microcrystallites were immobilized in pellets) with a Quantum Design MPMS-XL SQUID magnetometer between 2 and 300 K in applied magnetic field of 2 kOe in the 2-20

K temperature range and 10 kOe above 20 K. All the measurements were corrected for the diamagnetic contribution as calculated with Pascal's constants. The ac magnetic susceptibility measurements were performed on both Quantum Design MPMS-XL SQUID and Quantum Design PPMS magnetometers.

X-ray Crystallography

The SCXRD data for the compounds have been collected on a Bruker SMART CCD diffractometer (MoKα radiation, λ = 0.71073 Å). Collecting frames of data, indexing reflections, and determining lattice parameters was done by the program SMART, integrating the intensity of reflections and scaling was done by SAINT[12], SADABS[13] for absorption correction, and SHELXTL[14] for space group and structure determination and least-squares refinements on F^2. The crystal structures were solved and refined by full-matrix least-squares methods against F^2 by using the program SHELXL-2014[15] using Olex^2 software[16]. Some solvent molecules in **1** and **4** have been found to be highly disordered and have weak residual Q peaks. These were masked using Olex^2 program. The void volumes and the possible masked out electron counts have been included in the corresponding CIFs. All other non-hydrogen atoms were refined with anisotropic displacement parameters. The position of the hydrogen atoms were fixed at calculated positions and refined isotropically thoroughly. The crystallographic figures have been generated using Diamond 3.1e program[17]. The crystal data and the cell parameters for compounds **1**−**4** are summarized in Table 1. Crystallographic data (excluding structure factors) for the structures of compounds **1-4** have been deposited with the Cambridge Crystallographic Data Centre (CCDC no 1904649-1904652). Copies of the data can be obtained, free of charge, on application to CCDC, 12 Union Road, Cambridge CB2 1EZ, U.K.: http://www.ccdc.cam.ac.uk/cgi-bin/catreq.cgi, e-mail: data_request@ccdc.cam.ac.uk, or fax: +44 1223 336033.

Computational Details

All calculations were performed on the X-ray structure and the spin Hamiltonian parameters were calculated using CASSCF/NEVPT2 approach. We also compared our results with CASSCF/RASSI-SO/SINGLE_ANISO calculations. For this we have used ORCA 4.0 and MOLCAS 8.0 suit program.[18] Using ORCA suite state averaged complete-active space self-consistent field (CASSCF) wave functions was complemented by N electron valence second order perturbation theory (NEVPT2) to assess the role of dynamic correlation. The active space for the CASSCF involves 7 d electrons of the 5 3d orbitals [CAS9(7,5)]. For our calculations we have computed 10 quartets and 40 doublets states. The polarized triple-ζ-quality of DKH type basis set [DKH-def2-TZVP] was used for Co and Fe whereas for Y [Sapporo-DKH3-DZP-2012], for C, N, O and Cl DKH-def2-TZVP(-f) , for H DKH-def2-SVP was used. For the CASSCF step we have used TrafoStep RIMO approximation and for NEVPT2 RI-NEVPT2 approximation was utilised to speed up the calculations. The spin-orbit coupling was taken into accounts through QDPT approach and for the ZFS and g tensors the effective Hamiltonian approach were employed.[19] For MOLCAS 8 package we have gone through the CASSCF/RASSI/SINGLE_ANISO module of program. The same CAS space and roots were taken as mentioned earlier for the ORCA calculations. The basis set used were of ANO RCC type with triple zeta polarization. For carbon C. ANO-RCC...4s3p2d.,H.ANO-RCC...2s.,O.ANO-RCC...3s2p1d.,N.ANO-RCC...3s2p1d., cobalt Co. ANO-RCC...6s5p3d2f1g., yttrium Y.ANO-RCC...7s6p4d2f1g. The magnetic properties were obtained from the SINGLE_ANISO module.[20]

Synthesis

The ligand (H_2L) was synthesized by following a previously published method.[10]

Preparation of complexes 1, 3, 4

A general procedure for the synthesis of the complexes **1**, **3**, **4** is as follows. H_2L (0.053 mmol) was taken in a chloroform–methanol (30 mL, v/v, 1:1) mixture. To this, $Co(ClO_4)_2 \cdot 6H_2O$ (0.053 mmol) was added and stirred for 10 minutes followed by addition of $Y(NO_3)_3 \cdot xH_2O$(0.053 mmol) and then Et_3N (0.159 mmol). After stirring for another 10 minutes the corresponding acid, RCOOH (0.053 mmol) was added and the final solution was stirred for next 8 hours at room temperature. Removal of the solvent afforded a reddish solid which was washed by Et_2O followed by re-dissolution in CH_3CN-$CHCl_3$ (20 mL, v/v, 1:1), which produced suitable crystals for SCXRD upon slow evaporation.

Preparation of complex 2

To a (30 mL, v/v, 1:1) chloroform–methanol solution of LH_2 (0.053 mmol) was added Et_3N (0.106 mmol) followed by $Y(NO_3)_3 \cdot xH_2O$ (0.053 mmol) and the solution stirred for 10 minutes. After this $Co(OAc)_2 \cdot 4H_2O$ (0.053 mmol) was added at once and the solution heated to reflux for 3 h before the solvent was completely stripped off in vacuo, resulting in a red powder which was washed by Et_2O. Single crystals suitable for SCXRD were obtained by slow evaporation after dissolving the red powder in CH_3CN-$CHCl_3$ (20 mL, v/v, 1:1). Specific details of all corresponding reactions, yield and the characterization data of the complexes are given below.

$[Co(\mu\text{-}L)(\mu\text{-}CCl_3COO)Y(NO_3)_2] \cdot 2CHCl_3 \cdot CH_3CN \cdot 2H_2O$ (1)

Quantities: LH_2 (0.03g), $Y(NO_3) \cdot 6H_2O$ (0.0203 g), $Co(ClO_4)_2 \cdot 6H_2O$ (0.0195 g), CCl_3COOH (0.008 g),Et_3N (0.0161 g), yield: 0.038 g, 53.5% (based on Co^{2+}). M.P: > 260 °C. FT-IR (KBr) cm^{-1}: 3388 (b), 2942 (w), 1656 (s), 1606 (s), 1595 (s), 1511 (s), 1476 (s), 1361 (s), 1294 (s), 1220 (s), 842 (s), 742 (s). Anal. Calcd. for $C_{36}H_{40}Cl_9CoFeN_7O_{15}Y$ (1333.502): C, 32.42; H, 3.02; N, 7.35. Found: C, 32.68; H, 3.17; N, 7.54.

$[Co(\mu\text{-}L)(\mu\text{-}CH_3COO)Y(NO_3)_2] \cdot CH_3CN$ (2)

Quantities: LH_2(0.03g), $Y(NO_3)\cdot 6H_2O$ (0.0203 g),$Co(OAC)_2\cdot 4H_2O$ (0.013 g), Et_3N (0.0106 g), yield: 0.0289 g, 58% (based on Co^{2+}).M.P: > 260 °C. FT-IR (KBr) cm^{-1}: 3374 (b), 2936 (w), 2836 (w), 1668 (w), 1607 (s), 1464 (s), 1384 (s), 1297 (s), 1270 (s), 1219 (s). Anal. Calcd. for $C_{34}H_{37}CoFeN_7O_{13}Y$ (955.381): C, 42.74; H, 3.90; N, 10.26. Found: C, 42.68; H, 3.57; N, 10.54.

[Co(*μ*-L)(*μ*-PhCOO)Y(NO$_3$)$_2$]·3CH$_3$CN·2H$_2$O (3)

Quantities: LH_2 (0.03g), $Y(NO_3)\cdot 6H_2O$ (0.0203 g), $Co(ClO_4)_2\cdot 6H_2O$ (0.0195 g), PhCOOH (0.007 g), Et_3N (0.0161 g), yield: 0.0299 g, 49.5% (based on Co^{2+}).M.P: > 260 °C. FT-IR (KBr) cm^{-1}: 3388 (b), 2947 (w), 1607 (s), 1554 (s), 1467 (s), 1401 (s), 1297 (s), 1238 (s), 1220(w). Anal. Calcd. for $C_{43}H_{49}CoFeN_9O_{15}Y$ (1135.585): C, 45.48; H, 4.35; N, 11.1. Found: C, 45.68; H, 4.57; N, 11.04.

[Co(*μ*-L)(*μ*-^{t}BuCOO)Y(NO$_3$)$_2$]·CHCl$_3$·2H$_2$O (4)

Quantities: LH_2 (0.03g), $Y(NO_3)\cdot 6H_2O$ (0.0203 g), $Co(ClO_4)_2\cdot 6H_2O$ (0.0195 g), ^{t}BuCCOOH (0.005 g), Et_3N (0.0161 g), yield: 0.0335 g, 56.5% (based on Co^{2+}).M.P: > 260 °C. FT-IR (KBr) cm^{-1}: 3372 (b), 3124 (w), 2959 (w), 2320 (w), 1609 (s), 1559 (s), 1473 (s), 1423 (s), 1294 (s), 1238 (s), 1216 (s), 970 (s), 738(s). Anal. Calcd. For $C_{36}H_{45}Cl_3CoFeN_6O_{15}Y$ (1111.817): C, 38.89; H, 4.08; N, 7.57. Found: C, 38.61; H, 4.17; N, 7.24.

Results and Discussion

Synthesis

We have previously demonstrated the utility of ferrocene-supported ligands for the preparation of heterometallic 3d/4f complexes.[10] Thus, the ferrocene-based compartmental hexadentate LH_2 ligand comprises of two specific coordination pockets, an inner coordination pocket (P1, Scheme 1) composed of two imine nitrogen and two bridging phenoxy oxygens (N_2O_2) which specifically bind with 3d ions and an outer coordination pocket (P2, Scheme 1) consisting of

two phenoxy oxygens and two methoxy oxygen atoms (O_4 coordination environment) which preferentially bind to 4f metal ions. The reaction of LH_2 with $Co(OAc)_2{\cdot}4H_2O$ and $Y(NO_3)_3{\cdot}xH_2O$ in the presence of Et_3N as base in the molar ratio of 1:1:1:2 under reflux conditions yields the complex $[Co(\mu\text{-}L)(\mu\text{-}CH_3COO)Y(NO_3)_2]{\cdot}CH_3CN$ (**2)**; here the acetate ion acts as the bridging ligand linking the Co(II) and Y(III) metal ions. Under approximately similar reaction conditions the reaction of LH_2 with $Co(ClO_4)_2{\cdot}6H_2O$ and $Y(NO_3)_3{\cdot}xH_2O$ in the presence of trichloroacetic acid or benzoic acid or pivalic acid and Et_3N as the base in the stoichiometric ratio of 1:1:1:1: afforded the complexes, $[Co(\mu\text{-}L)(\mu\text{-}CCl_3COO)Y(NO_3)_2]{\cdot}2CHCl_3{\cdot}CH_3CN{\cdot}2H_2O$ **(1),** $[Co(\mu\text{-}L)(\mu\text{-}PhCOO)Y(NO_3)_2]{\cdot}3CH_3CN{\cdot}2H_2O$ **(3)** $[Co(\mu\text{-}L)(\mu\text{-}^tBu_3COO)Y(NO_3)_2]{\cdot}CHCl_3{\cdot}2H_2O$ (**4)** respectively (Scheme 1). All the complexes possess a similar type of core and only differ in the number/nature of solvent molecules of crystallization.

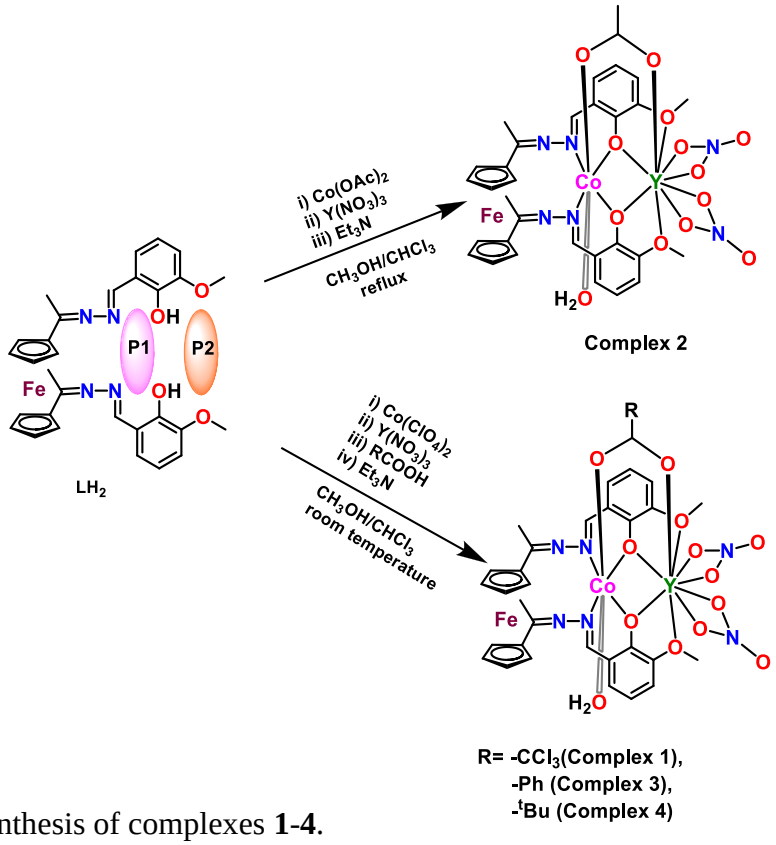

Scheme 1. Synthesis of complexes **1**-**4**.

For investigating the structural integrity of the **1**–**4** in solution, we have carried out ESI–MS studies which revealed parent ion peaks for corresponding complexes, although in lower abundance relative to other fragments. A representative ESI-MS spectrum of **1** is given in Figure 1 while spectra for the rest of the complexes are given in the Supporting Information. Interestingly, all the complexes, **1**-**4,** show a distinct peak with very high abundance at around m/z = 802. This is presumably due to the common dinuclear fragment, $[Co(\mu\text{-}L)Y(OEt)_2]^+$, independent of the nature of the bridging ligand present in these complexes.

(a) (b)

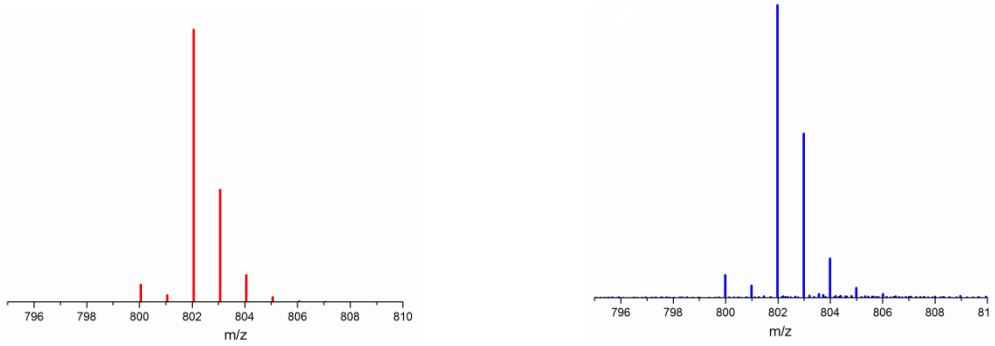

Figure 1. ESI-MS of $[Co(\mu\text{-}L)Y(OEt)_2]^+$ (fragment) (a) theoretical simulation (red lines); (b) experimental spectrum simulated (blue lines) for complex **1**.

X-ray Crystallography

Among the four heterometallic dinuclear $Co^{II}Y^{III}$ complexes, **1**, **2** and **4** crystalized in the triclinic *P*-1 space group while complex **3** crystallized in the monoclinic $P2_1/c$ space group. In view of the structural similarity of the complexes, **2** is taken as a representative example to describe the structural features of this dinuclear complexes family.

In complex **2** the Co^{II} center occupies the inner coordination pocket P1 of the ligand with a 2N, 4O coordination environment. The coordinating atoms involved are as follows: two nitrogen atoms, N1 and N2, from the imine part of the ligand [Co-N1, 2.162(3) Å; Co-N2, 2.109(3) Å]; two phenoxide oxygen atoms O4 and O5 of the ligand [Co-O4, 2.062(2) Å; Co-O5, 2.083(2) Å]; one oxygen atom O1 from the bridging carboxylate ligand [Co-O1, 2.032(2) Å]; finally O3 from water molecule [Co-O3, 2.123(2) Å]. The overall coordination geometry around Co^{II} can be described as distorted octahedral geometry. The coordination environment around Y^{III} is 9O and the coordination geometry can be described by the continuous SHAPE analysis[21] to be Muffin-shaped (MFF-9) in *Cs* symmetry. The Y^{III} ion is ensconced in the outer coordination pocket P2 of the ligand. The total coordination arrangement around Y^{III} ion occurs in the

following manner: two bridging phenoxide oxygen atoms O4 and O5 [Y-O4, 2.282(2) Å; Y-O5, 2.083(2) Å]; one oxygen atom O2 from the bridging carboxylate group [Y-O2, 2.284(2) Å]; four oxygen atoms O7, O8, O9 and O10 from two chelating nitrate groups [Y-O7, 2.438(2) Å; Y-O8, 2.478(2) Å; Y-O9, 2.399(2) Å; Y-10, 2.435(3) Å] and two oxygen atoms O6 and O11 from two methoxy groups of the ligand [Y-O6, 2.533(2) Å; Y-O11, 2.606(2) Å].

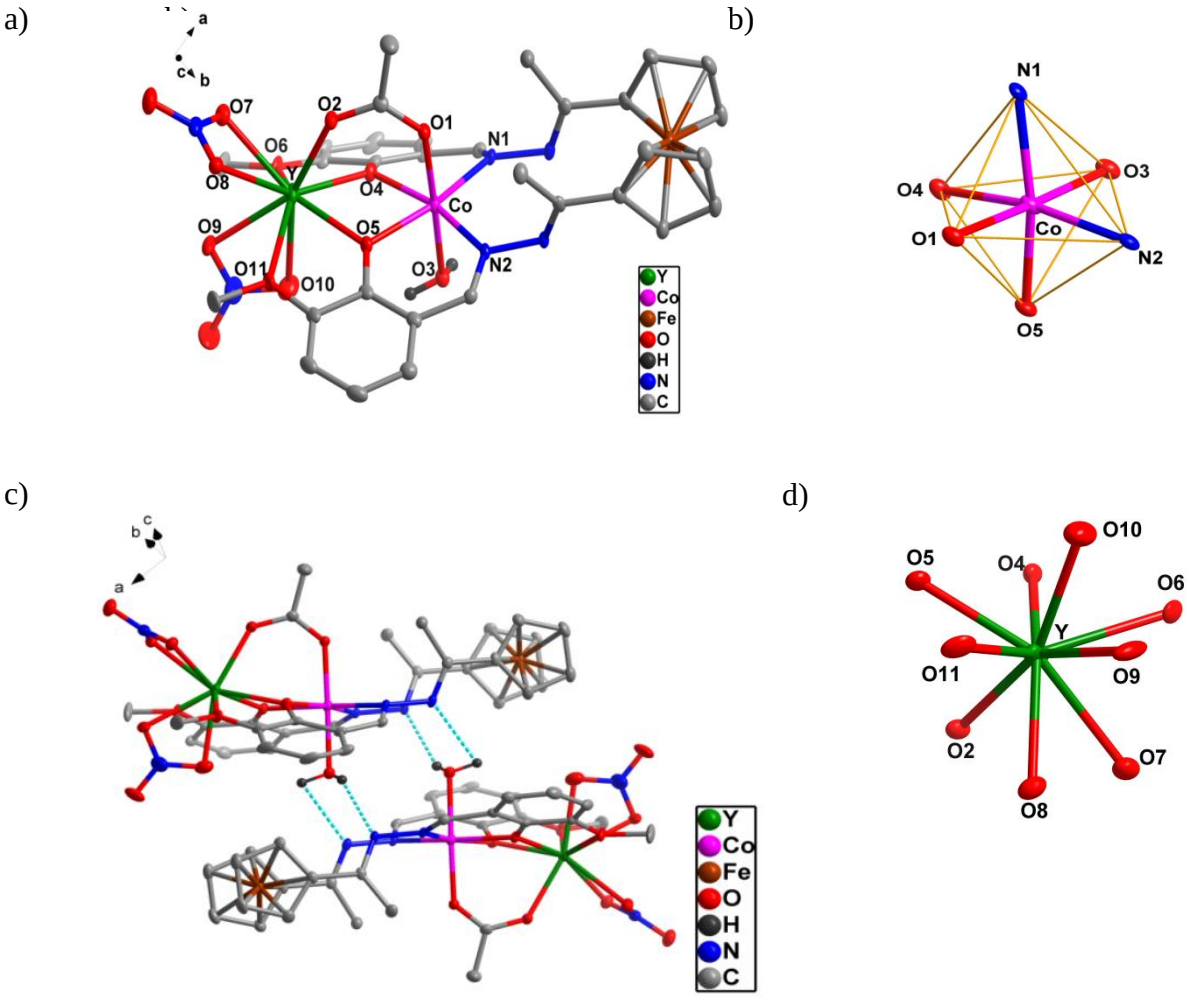

Figure 2. a) Full molecular structure of **2** (selected hydrogen atoms and solvent molecules are removed for the sake of clarity) ; b) distorted octahedral geometry around the Co^{II} ion; c) two molecules of complex **2** showing intermolecular hydrogen bonding (light blue colored dotted

bonds), d) coordination environment around the Y^{III} ion. Ellipsoids are drawn at 40 % probability for non-metallic atoms and at 50 % probability for metallic atoms.

The phenoxide bridging action between the Co^{II} and Y^{III} centers results in a $CoYO_2$ four-membered ring (see Figure S6). Within this ring it is interesting to note that the two Y-O-Co bridging angles (Co-O4-Y and Co-O5-Y) are not the same in all the complexes. Also it is worth mentioning that the O4-Co-O5 angle is always greater than the O4-Y-O5 angle for each complex.

As the nature of the bridging carboxylate groups are different in each complex, in spite of the overall structural similarity, certain small but subtle differences are noticed in the four complexes. The obtained CShM values from continuous SHAPE measurement[21] for OC6↔TPR6 deformation pathway show that the structures are much closer to the OC-6 geometry (see Table 1) and reveals that the degree of distortion continuously increases from **1** to **4** regularly.

Table 1. CShM values obtained from continuous SHAPE analysis for complex **1**-**4**

Complex	Complex **1**	Complex **2**	Complex **3**	Complex **4**
CShM value for the OC-6 polyhedron	0.758	0.763	0.800	0.859

The differences in crystallographic parameters around the Co^{II} center that are summarized in the Table 2 also act in support of the difference in distortion from perfect geometry among the complexes.

Table 2. Selected bond parameters for complexes **1**-**4**

Bond/Angle description	Complex **1**	Complex **2**	Complex **3**	Complex **4**
Co-O1	2.099(64)	2.032(23)	2.073(49)	2.067(26)
Co-O3	2.111(64)	2.123(24)	2.153(55)	2.125(29)
Co-O4	2.071(47)	2.061(23)	2.075(51)	2.082(2)
Co-O5	2.079(5)	2.083(22)	2.062(56)	2.069(2)
Co-N1	2.135(69)	2.162(25)	2.136(73)	2.138(27)
Co-N2	2.124(64)	2.109(26)	2.137(71)	2.147(23)
O1-Co-O3	176.294(22)	177.093(94)	177.426(2)	177.946(98)
O1-Co-O4	88.866(21)	88.826(92)	90.461(2)	89.624(92)
O1-Co-O5	88.386(22)	89.017(9)	88.325(2)	88.938(88)

Colacio *et. al.* previously reported two sets {(**1a**,**1b**,**1c**)[7a] and **2a**[7b]}of $Co^{II}Y^{III}$ complexes (Figure 3) that also have distorted octahedral Co^{II} and nine-coordinated Y^{III} centers.. The bond parameters observed in the present instance are consistent with these literature precedents.

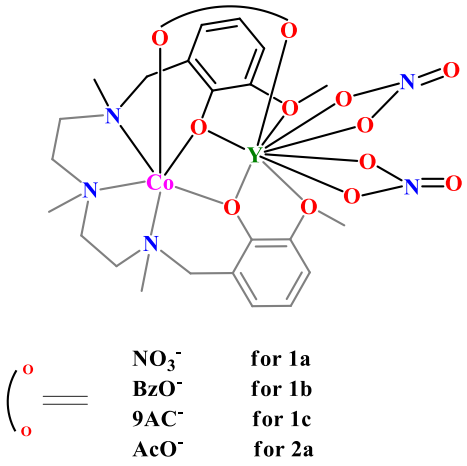

Figure 3: Compounds **1a**, **1b**, **1c** and **2b** known in literature.[7]

Magnetic Properties

The thermal variations of $\chi_M T$ (χ_M, the molar magnetic susceptibility; T, the temperature in Kelvin), for the four compounds are very similar. Thus, the $\chi_M T$ is around 3 cm^3 K mol^{-1} at room temperature and monotonically decreases on cooling down to reach 1.84, 1.63, 1.68 and 1.51 cm^3 K mol^{-1} for compounds **1** to **4** at 2 K, respectively (Figure 4). The room temperature values are much higher than expected for isolated S = 3/2 with g = 2.0 (1.875 cm^3 K mol^{-1}) but match with the commonly accepted values for high spin octahedral Co(II) with spin orbit coupling in the orbitally degenerate ground state $^4T_{1g}$ and distortions of the octahedral coordination sphere.[22] The low temperature values also match with the stabilization of a S_{eff} = 1/2 effective spin with g_{eff} close to the 4.33 value expected in the absence of distortion.[19] The first magnetization curves at 2 K are represented also on Figure 4. They tend to saturate at values close to 2.2 Nβ for all compounds in agreement with the expected value of 2.165 Nβ for the effective spin ½ with g = 4.33.

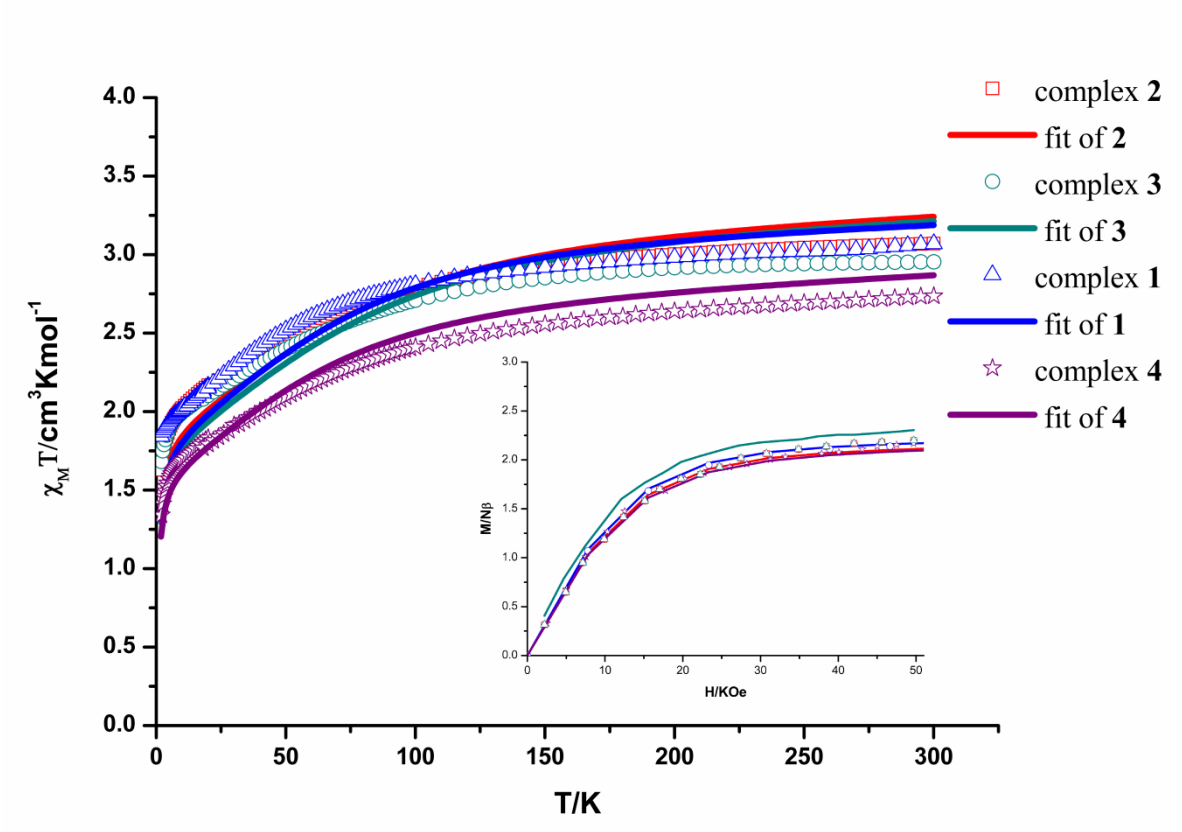

Figure 4. Thermal variation of $\chi_M T$ with the first magnetization curves at 2 K for **1-4** in the inset. The $\chi_M T$ and the magnetization experimental values are fitted using PHI software with the NEVPT2 calculated D and E parameters.

None of the four compounds display an out-of-phase signal of the ac magnetic susceptibility, χ_M'', in the absence of an external dc field down to 2 K in the frequency range $\nu = 1 \rightarrow 10000$ Hz of the oscillating field because of possible quantum tunneling of the magnetization (QTM). However, such QTM can be suppressed by the application of a moderate external dc field inducing a slowing down of the relaxation of the magnetic moment of Co^{II}. It is characterized by the appearance of a maximum on the χ_M'' vs. ν curves between 100 and 1000 Hz for compounds **1**, **3** and **4** while the maximum is located at higher frequency (>1000 Hz) for **2** (Figure S8). It is not the only major difference between the four compounds. Indeed, for **1** a "so-called" optimum field (the field for which the relaxation is the slowest) is clearly visible around 1200 Oe with an amount of relaxing matter (the amplitude of χ_M'' near the maximum) almost constant above 500 Oe while for **3** and **4** the relaxation accelerates continuously with the field and the amplitude of χ_M'' increases. Compound **2** seems to behave similarly to **3** and **4** with however the maximum which potentially falls at higher frequencies than 1000 Hz.

The four compounds were studied under an applied magnetic field of 1200 Oe. All the compounds displayed strong frequency dependence of the magnetic susceptibility between 2 and 15 K (Figures 5 and S8).

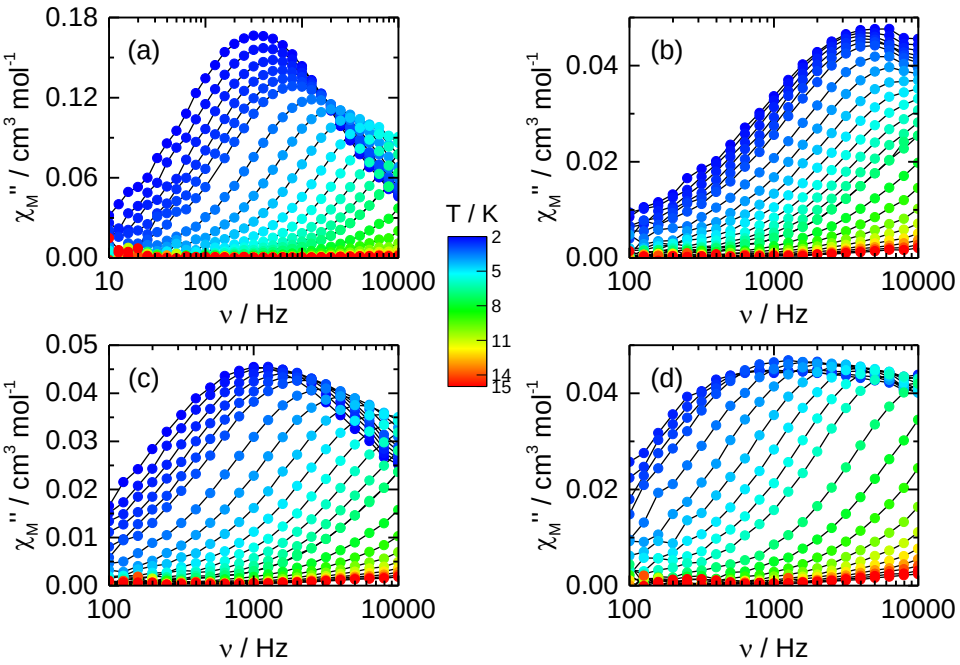

Figure 5. Frequency dependence of χ_M'' between 2 and 10 K for compounds **1-4** (a to d, respectively) under a 1200 Oe applied magnetic field.

The AC data for **1-3** were fit in the framework of the extended Debye model[23,24] for a single relaxation process with a distribution (α) of relaxation times (τ) (Table S1-S3) while for **4** the frequency maxima are manually selected due to the large out-of-phase signal of the magnetization at low temperature (Figure 5d). The high temperature part of the log(τ) versus T curves seems to follows the Arrhenius law $\tau = \tau_0 \exp(\Delta/kT)$ with $\tau_0 = 3.2(4)\times10^{-6}$ s and Δ = 8.4(6) K for **1**, $\tau_0 = 2.5(2)\times10^{-6}$ s and Δ = 11.0(4) K for **2**, $\tau_0 = 2.6(4)\times10^{-6}$ s and Δ = 13.7(8) K for **3** and $\tau_0 = 7.4(9)\times10^{-7}$ s and Δ = 18.7(6) K for **4** (Figure S9). The thermal dependence plots of the relaxation time clearly show a deviation from the linearity below 4 K a sign of other operative relaxation mechanisms. The much lower experimental energy barrier of the four compounds compared to the calculated values (301.1 K, 256.2 K, 303.6 K and 222.6 K respectively for **1-4** compounds) is an indication of a negligible contribution of the Orbach process with respect to Raman, QTM and Direct relaxations. Magnetic relaxation through

Direct mechanism can be observed on the scan field of the magnetic susceptibility for **2** and **3** since increasing the magnetic field value induced shift to the χ_M" maxima at higher frequency (Figure S7). Therefore, the log(τ) versus T curves in 2-6 K can be analyzed using the following expression:

$$\tau^{-1} = ATH^4 + CT^n + \tau_{TI}^{-1}$$

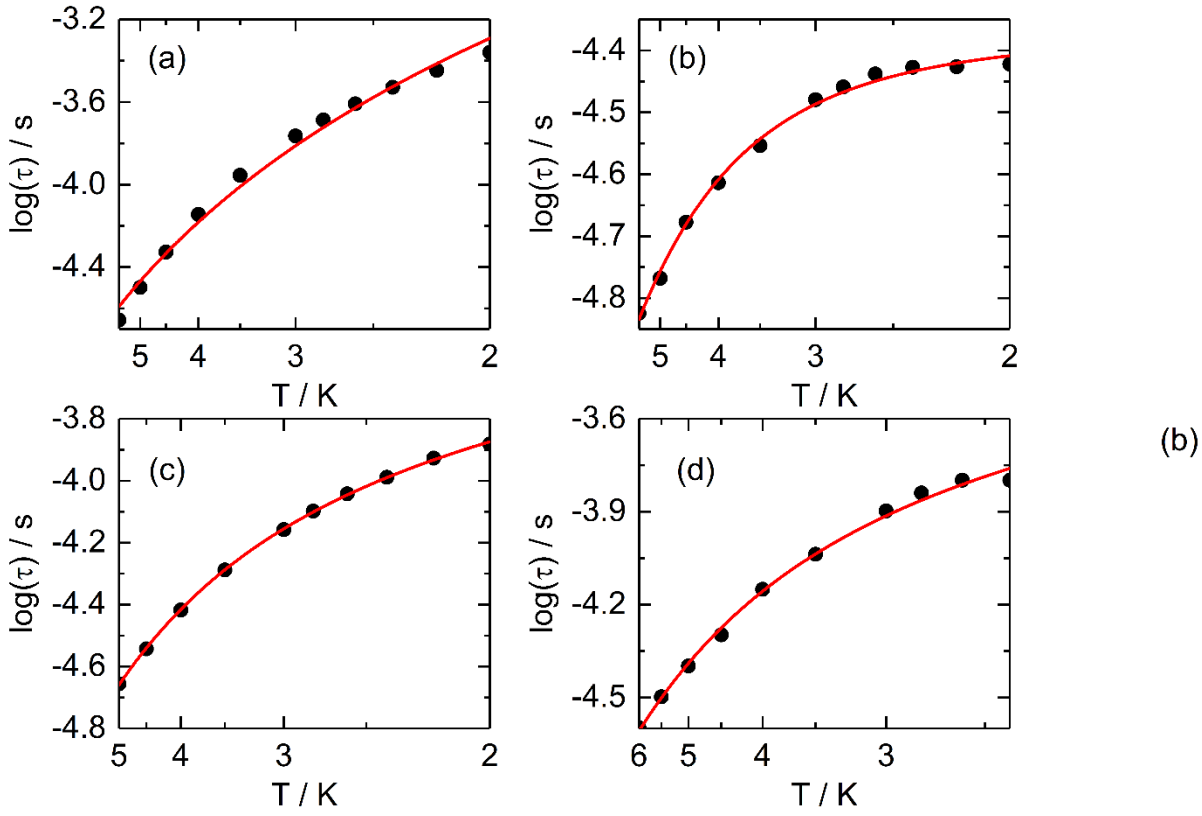

Figure 6. Arrhenius plots of the relaxation times in 1200 Oe applied magnetic field for **1**-**4** (a to d, respectively) (black disks). Full red lines are the best-fit curves (see text).

The best fit for compounds **2**-**3** were obtained using the combination of Raman and Direct processes as reported by E. Colacio and coll.[7a] for similar $Co^{II}Y^{III}$ compounds with the parameters depicted in Table 3. On contrast the best fit for 4 was obtained by the combination of Raman and remaining QTM while **1** was obtained using a pure Raman process (Table 3).

For the latter the absence of QTM is explained by the AC measurements under the optimal field of 1200 Oe while for **2**-**4** the optimal magnetic field value cannot be reached.

Table 3. Fitting parameters with associated errors given in brackets for **1**-**4**.

	1	**2**	**3**	**4**
C ($s^{-1}K^{-n}$)	252 (30)	90 (16)	37 (29)	154 (51)
n	2.96(10)	3.6(1)	3.7(4)	3.06(19)
τ_{QTM} (s)	/	/	/	$2.74(37)\times10^{-4}$
A ($s^{-1}K^{-m}$) *M fixed to 4*	/	$1.54(4) \times 10^{-9}$	$9.6(10) \times 10^{-10}$	/

The extracted values for the n parameter are in agreement with those expected for Kramers ions when both optical and acoustic phonons (n = 1-6) are involved in the relaxation mechanism.[25] As a consequence, **1** is the slowest and **2** is the fastest with **4** and **3** the intermediates.

Theoretical Studies

To illustrate various experimental observations and also to probe the origin of the slow relaxation in the presence of field, we have undertaken a detailed *ab initio* calculations using two approaches (see computational details for further information). The computed spin Hamiltonian parameters are given in Table 4 and the estimated values are in general agreement with the values obtained from experiments. The estimated axial (rhombic) ZFS parameters, D (E), are given in Table 4 for complexes **1**-**4**. The E/D values are significant and this corroborate well with larger E values. The values obtained from NEVPT2 calculations are very similar to the values obtained from CASSCF and also using MOLCAS (see Table 4 in ESI, also see

Figure S11 and S12 in the ESI for computed D orientation with respect to the molecular framework). Positive D obtained for all complexes is in agreement with the experiments where relaxation is observed only in the presence of an applied field.[4, 26] Additionally such a large computed D value suggests that the system can be described using a pseudo spin ½ system. Using pseudo-spin ½ estimates the low temperature limit of $\chi_M T$ can be calculated: 2.06, 2.02, 2.12 and 1.88 cm^3 K mol^{-1} for **1** to **4**, respectively. These values are in relatively good agreement with the experiment and also corroborated by the saturation values of the magnetization recorded at 2 K which match the expected 2.2, 2.18, 2.07 and 2.13 Nβ for **1** to **4**, respectively. Additionally we have simulated the susceptibility and the magnetization data for these complexes using the *ab initio* estimated parameters and very good match has been found offer confidence on the estimated parameters.

Table 4. Estimated D, E and g-tensors for **1**-**4** using *ab initio* calculations.

Complexes	CASSCF/RASSI-SO		NEVPT2		g_x	g_y	g_z
	D_{cal}/cm^{-1}	E_{cal}/cm^{-1}	D_{cal}/cm^{-1}	E_{cal}/cm^{-1}			
1	101.9	13.7	87.9	11.6	7.075	3.105	2.178
2	88.8	3.5	91.7	23.0	6.984	3.227	2.198
3	93.8	27.9	90.0	18.5	7.296	2.932	2.026
4	76.8	5.4	72.4	18.3	7.218	2.881	1.955

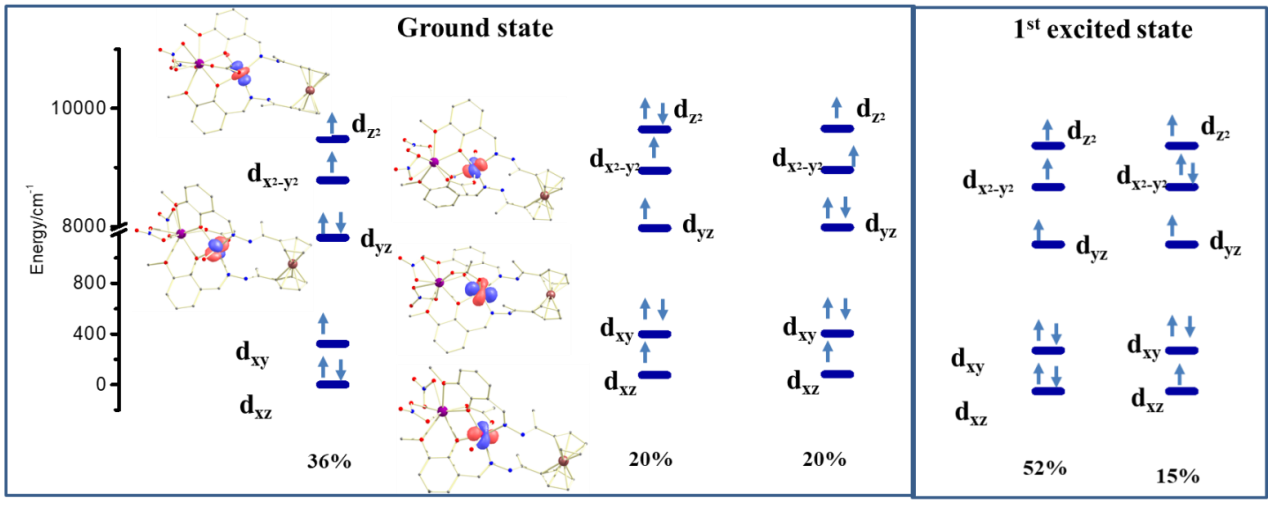

Figure 7. Orbital energies computed for the ground and first excited state of complex **2**. The percentage mention reveals the % of the corresponding configuration mixing.

The ground state electronic configuration for the Co(II) ion is found to be strongly multi-determinantal in characteristics for all four complexes. For example in complex **2**, the ground state has $(d_{xz})^2(d_{xy})^1(d_{yz})^2(d_{x2-y2})^1(d_z^2)^1$ configuration that is dominant (36%) and is mixed strongly with other two states with the weightage of 20% (See Figure 7). This is expected for the six-coordinate Co(II) possessing unquenched orbital contribution leading to larger D values. The dominant contribution to the positive D value is found to arise from the two close lying quartet states, particularly the first quartet state is found to contribute more than 50% to the net D value for all four complexes. The first excited state is also found to be multi-determinantal in character with strong mixing and transition from $d_{xz} \rightarrow d_{xy}$ orbital found to contribute significantly to the total D value. As the two orbitals involved have different m_l levels, the sign of D is found to be positive for all four complexes.[27]

Since the first excited state contributes significantly to the D value, the gap between the ground to the first excited state is strongly correlated to the magnitude of D value. The trend in the computed D is found to be **2**>**3**>**1**>**4** with the D value computed for complex **4** found to be smaller than other three complexes. The magnitude of the computed D is found to correlate with the ground to first and second excited states which are the dominant contributor to the D value. The energies computed for the first and second excited states along with their contribution to the D values are given in Figure 8 and Supporting Information. Particularly for complex **4** both the first and second excited quartet states are strongly destabilized compared to complexes **1**-**3** leading to a smaller D value.

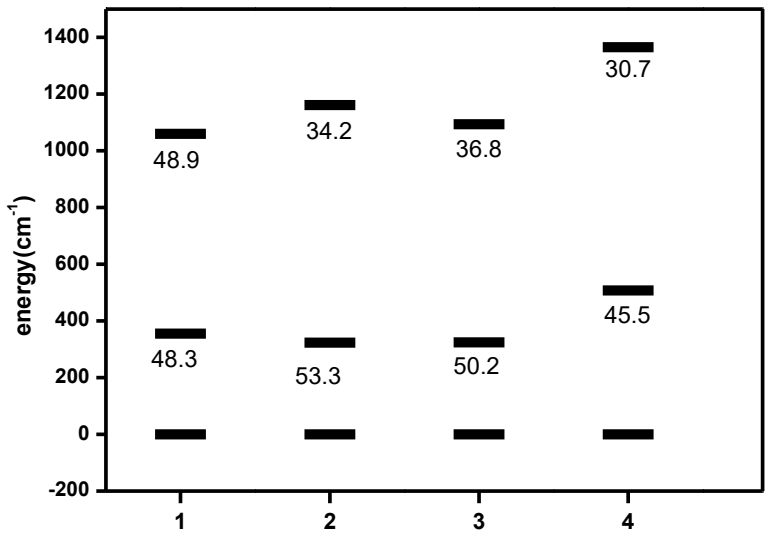

Figure 8. The energy gap between the ground, first and second excited quartet states computed for complexes **1**-**4**. The numbers mentioned below the line reveal the contribution to the D value by that particular state (in cm^{-1}).

The computed g-tensors for complexes **1-4** are given in Table 4. Clearly, as we expected for a positive D value, the g_{xx} values are found to be much larger than g_{zz}. Due to the low symmetry of the complexes the g_{zz} and D_{zz} axes are found to be non-coincident for these complexes (see Figures 9 and S11 and S12). This low symmetry leads to significant E value for all the four complexes and this is reflected in the E/D value, where a high value indicates the rhombic nature of the transverse anisotropy leading to non-coincidence of the D_{zz} and g_{zz} axes.

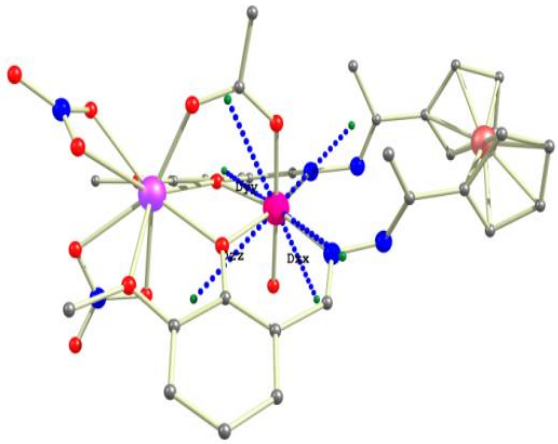

Figure 9. Computed orientation of D_{zz} and g_{zz} axes for complex **1**.

The $d_{xz} \rightarrow d_{xy}$ transition is the prime contributor to the positive D and the computed trend for the magnitude of D among complexes **1**-**4** is also reflected in the contribution arising from the first excited state (i.e. **2**>**3**>**1**>**4**). Qualitatively the first excited state reflects the energy gap between the d_{xz} and d_{xy} orbitals. Since the d_{xy} orbital is orthogonal to the acetate bridge, its energy is expected to be only marginally influenced by the substitution in the acetate group, however the energy of the d_{xz} orbital is significantly influenced as this orbital has a weak π^* antibonding interaction with the acetate oxygen atom. The substitution at the acetate position tends to stabilize or destabilize the d_{xz} orbital leading to a variation in the d_{xz} to d_{xy} gap and hence the variation in the magnitude of D value among complexes **1**-**4**.

EPR Studies

To have a clear idea on the sign of D we have recorded Q-band EPR spectra of these complexes on powder samples of **2**-**4** (Figure S14). All the recorded EPR spectra were characteristics of high spin Co^{II} (S=3/2) with very high positive ZFS parameter D as no transition were observed for $m_s=\pm1/2$ to $m_s=\pm3/2$ levels since the energy gap between the two levels are much higher (consistent with values obtained from the CASSCF and NEVPT2 results, 150 cm^{-1} to 210 cm^{-}

[1]) and validate the pseudo-spin approximation that was adapted as discussed earlier. The recorded EPR spectra are very similar to the EPR data reported earlier for the octahedral Co(II) complexes possessing positive D and offer confidence on the estimated parameters.[ref]

The observed transition could be attributed to the transition between the m_s=±1/2 levels, hence the m_s=±1/2 is the ground state suggesting positive D. For D< 0 case, the low lying state is KD=±3/2 and the transition within these states are generally less visible in the recorded frequency leading to absence of any features in the EPR spectra.[7]

To further understand the nature of the EPR spectra we have simulated the EPR spectra of complex **3** using NEVPT2 estimated D, E and g-values and with minor perturbations to the g-tensors. Many of the experimental features are reproducible offering confidence on the sign of the assigned D.

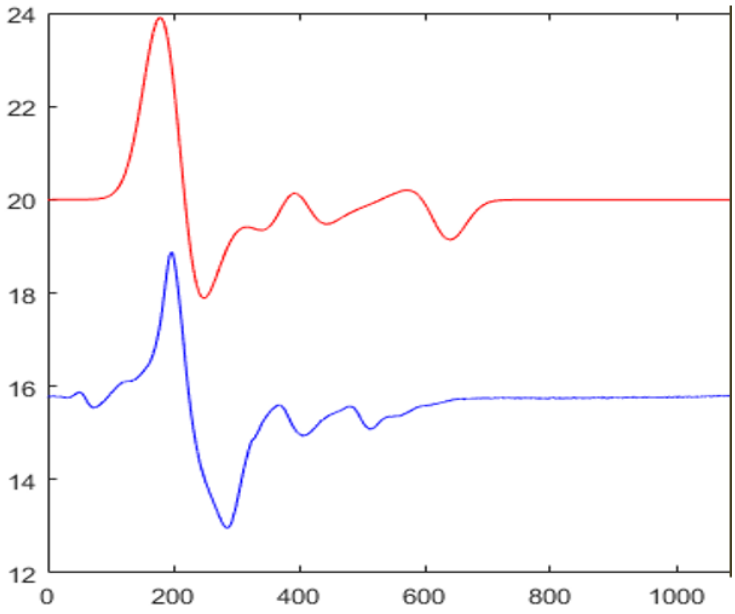

Figure 10. Experimental and simulated Q-band EPR spectra for complex **3**. Blue= Experimental, Red= simulated. Simulation is performed using the following set of spin Hamiltonian parameter D = 93 cm^{-1}, E/D =0.3, g_{xx} =4.8, g_{yy}=2.93, g_{zz}=1.8 and Line width 65.

Conclusion

Proper understanding of the relations between geometric and electronic structure with magnetic properties are still a wide field left to be covered well. In this work we have synthesized four $Co^{II}Y^{III}$ systems in a targeted way by altering different acetate bridging ligand. With the help of these four molecules we have tried to explore how the electronic properties of the bridging acetate ligands in the $Co^{II}Y^{III}$ systems controls the magnetic anisotropy as well the magnetic slow relaxation. The six coordinated distorted octahedral geometry around the Co^{II} center within the molecules dictates the molecule to show a field induced magnetic relaxation. The extracted energy barriers for the high temperature region for the molecules are seen to be dependent on the nature of the bridging ligand. *Ab initio* calculation showed that all the molecules have positive D values which is largely due to the contribution of the transition from d_{xz} to d_{xy} orbitals for the molecules. Also it was calculated that although the effect of bridging ligand on d_{xy} orbital is not so prominent but the d_{xz} orbital is in direct interaction with the π^*orbital of the O atoms of the bridging ligand. So subtle changes in the electronic properties on the bridging ligands stabilize or destabilize the d_{xz} orbital leading to a variation in the magnitude of D value for the complexes **1**-**4**.

Acknowledgement

We thank the Department of Science and Technology (DST), India, the CNRS, Université de Rennes 1, the European Commission through the ERC-CoG 725184 MULTIPROSMM (project n. 725184) for financial support, also support for a Single Crystal CCD X-ray Diffractometer facility at IIT-Kanpur. V.C. is grateful to the DST for J. C. Bose fellowship. J.A. thanks Department of Science and Technology (DST), India for INSPIRE Senior Research Fellowship. GR would like to than SERB for funding (CRG/2018/000430) and IITB multi-frequency EPR facility for recording the EPR spectra.

References

1. (a) Hill, S.; Edwards, R. S.; Aliaga-Alcalde, N.; Christou, G., Quantum Coherence in an Exchange-Coupled Dimer of Single-Molecule Magnets. *Science* **2003**, *302* (5647), 1015-1018; (b) Leuenberger, M. N.; Loss, D., Quantum computing in molecular magnets. *Nature* **2001,** *410*, 789.

2. (a) Craig, G. A.; Sarkar, A.; Woodall, C. H.; Hay, M. A.; Marriott, K. E. R.; Kamenev, K. V.; Moggach, S. A.; Brechin, E. K.; Parsons, S.; Rajaraman, G.; Murrie, M., Probing the origin of the giant magnetic anisotropy in trigonal bipyramidal Ni(ii) under high pressure. *Chem. Sci.* **2018**, *9* (6), 1551-1559; (b) El-Khatib, F.; Cahier, B.; López-Jordà, M.; Guillot, R.; Rivière, E.; Hafez, H.; Saad, Z.; Girerd, J.-J.; Guihéry, N.; Mallah, T., Design of a Binuclear Ni(II) Complex with Large Ising-type Anisotropy and Weak Anti-Ferromagnetic Coupling. *Inorg. Chem.* **2017,** *56* (17), 10655-10663; (c) Freedman, D. E.; Harman, W. H.; Harris, T. D.; Long, G. J.; Chang, C. J.; Long, J. R., Slow Magnetic Relaxation in a High-Spin Iron(II) Complex. *J. Am. Chem. Soc.* **2010,** *132* (4), 1224-1225; (d) Novikov, V. V.; Pavlov, A. A.; Nelyubina, Y. V.; Boulon, M.-E.; Varzatskii, O. A.; Voloshin, Y. Z.; Winpenny, R. E. P., A Trigonal Prismatic Mononuclear Cobalt(II) Complex Showing Single-Molecule Magnet Behavior. *J. Am. Chem. Soc.* **2015,** *137* (31), 9792-9795; (e) Rechkemmer, Y.; Breitgoff, F. D.; van der Meer, M.; Atanasov, M.; Hakl, M.; Orlita, M.; Neugebauer, P.; Neese, F.; Sarkar, B.; van Slageren, J., A four-coordinate cobalt(II) single-ion magnet with coercivity and a very high energy barrier. *Nat. Commun.* **2016,** *7*, 10467; (f) Shao, F.; Cahier, B.; Rivière, E.; Guillot, R.; Guihéry, N.; Campbell, V. E.; Mallah, T., Structural Dependence of the Ising-type Magnetic Anisotropy and of the Relaxation Time in Mononuclear Trigonal Bipyramidal Co(II) Single Molecule Magnets. *Inorg. Chem.* **2017,** *56* (3), 1104-1111; (g) Vaidya, S.; Tewary, S.; Singh, S. K.; Langley, S. K.; Murray, K. S.; Lan, Y.; Wernsdorfer, W.; Rajaraman, G.;

Shanmugam, M., What Controls the Sign and Magnitude of Magnetic Anisotropy in Tetrahedral Cobalt(II) Single-Ion Magnets? *Inorg. Chem.* **2016,** *55* (19), 9564-9578; (h) Zadrozny, J. M.; Xiao, D. J.; Atanasov, M.; Long, G. J.; Grandjean, F.; Neese, F.; Long, J. R., Magnetic blocking in a linear iron(I) complex. *Nat. Chem.* **2013,** *5*, 577; (i) Bunting, P. C.; Atanasov, M.; Damgaard-Møller, E.; Perfetti, M.; Crassee, I.; Orlita, M.; Overgaard, J.; van Slageren, J.; Neese, F.; Long, J. R., A linear cobalt(II) complex with maximal orbital angular momentum from a non-Aufbau ground state. *Science* **2018,** *362* (6421), eaat7319.

3. (a) Díaz-Torres, R.; Menelaou, M.; Roubeau, O.; Sorrenti, A.; Brandariz-de-Pedro, G.; Sañudo, E. C.; Teat, S. J.; Fraxedas, J.; Ruiz, E.; Aliaga-Alcalde, N., Multiscale study of mononuclear CoII SMMs based on curcuminoid ligands. *Chem. Sci.* **2016**, *7* (4), 2793-2803; (b) Herchel, R.; Váhovská, L.; Potočňák, I.; Trávníček, Z., Slow Magnetic Relaxation in Octahedral Cobalt(II) Field-Induced Single-Ion Magnet with Positive Axial and Large Rhombic Anisotropy. *Inorg. Chem.* **2014,** *53* (12), 5896-5898; (c) Korchagin, D. V.; Palii, A. V.; Yureva, E. A.; Akimov, A. V.; Misochko, E. Y.; Shilov, G. V.; Talantsev, A. D.; Morgunov, R. B.; Shakin, A. A.; Aldoshin, S. M.; Tsukerblat, B. S., Evidence of field induced slow magnetic relaxation in cis-$[Co(hfac)_2(H_2O)_2]$ exhibiting tri-axial anisotropy with a negative axial component. *Dalton Trans.* **2017,** *46* (23), 7540-7548; (d) Palii, A. V.; Korchagin, D. V.; Yureva, E. A.; Akimov, A. V.; Misochko, E. Y.; Shilov, G. V.; Talantsev, A. D.; Morgunov, R. B.; Aldoshin, S. M.; Tsukerblat, B. S., Single-Ion Magnet $Et_4N[Co^{II}(hfac)_3]$ with Nonuniaxial Anisotropy: Synthesis, Experimental Characterization, and Theoretical Modeling. *Inorg. Chem.* **2016,** *55* (19), 9696-9706; (e) Sertphon, D.; Murray, K. S.; Phonsri, W.; Jover, J.; Ruiz, E.; Telfer, S. G.; Alkaş, A.; Harding, P.; Harding, D. J., Slow relaxation of magnetization in a bis-mer-tridentate octahedral Co(ii) complex. *Dalton Trans.* **2018,** *47* (3), 859-867; (f) Vallejo, J.; Castro, I.; Ruiz-García, R.; Cano, J.; Julve, M.; Lloret, F.; De Munno, G.; Wernsdorfer, W.; Pardo, E., Field-Induced Slow Magnetic Relaxation in a Six-Coordinate

Mononuclear Cobalt(II) Complex with a Positive Anisotropy. *J. Am. Chem. Soc.* **2012,** *134* (38), 15704-15707.

4. Gómez-Coca, S.; Urtizberea, A.; Cremades, E.; Alonso, P. J.; Camón, A.; Ruiz, E.; Luis, F., Origin of slow magnetic relaxation in Kramers ions with non-uniaxial anisotropy. *Nat. Commun.* **2014,** *5*, 4300.

5. Chandrasekhar, V.; Pandian, B. M.; Azhakar, R.; Vittal, J. J.; Clérac, R., Linear Trinuclear Mixed-Metal Co^{II}–Gd^{III}–Co^{II} Single-Molecule Magnet: $[L_2Co_2Gd][NO_3]\cdot 2CHCl_3$ (LH_3 = (S)P[N(Me)NCH−C_6H_3-2-OH-3-OMe]$_3$). *Inorg. Chem.* **2007,** *46* (13), 5140-5142.

6. (a) Gómez, V.; Vendier, L.; Corbella, M.; Costes, J.-P., Tetranuclear $[Co–Gd]_2$ Complexes: Aiming at a Better Understanding of the 3d-Gd Magnetic Interaction. *Inorg. Chem.* **2012,** *51* (11), 6396-6404; (b) Goura, J.; Chakraborty, A.; Walsh, J. P. S.; Tuna, F.; Chandrasekhar, V., Hexanuclear 3d–4f Neutral $Co^{II}_2Ln^{III}_4$ Clusters: Synthesis, Structure, and Magnetism. *Cryst. Growth Des.* **2015,** *15* (7), 3157-3165; (c) Modak, R.; Sikdar, Y.; Thuijs, A. E.; Christou, G.; Goswami, S., Co^{II}_4, Co^{II}_7, and a Series of $Co^{II}_2Ln^{III}$ (Ln^{III} = Nd^{III}, Sm^{III}, Gd^{III}, Tb^{III}, Dy^{III}) Coordination Clusters: Search for Single Molecule Magnets. *Inorg. Chem.* **2016,** *55* (20), 10192-10202; (d) Radu, I.; Kravtsov, V. C.; Ostrovsky, S. M.; Reu, O. S.; Krämer, K.; Decurtins, S.; Liu, S.-X.; Klokishner, S. I.; Baca, S. G., Tetranuclear $\{Co^{II}_2Co^{III}_2\}$, Octanuclear $\{Co^{II}_4Co^{III}_4\}$, and Hexanuclear $\{Co^{III}_3Dy^{III}_3\}$ Pivalate Clusters: Synthesis, Magnetic Characterization, and Theoretical Modeling. *Inorg. Chem.* **2017,** *56* (5), 2662-2676; (e) Reu, O.; Palii, A.; Ostrovsky, S.; Wallace, W.; Zaharko, O.; Chandrasekhar, V.; Clerac, R.; Klokishner, S., Experimental Characterization and Theoretical Modeling of a Linear $[Co^{II}_2Tb^{III}]$ Single Molecule Magnet. *J. Phys. Chem. C* **2013,** *117* (13), 6880-6888.

7. (a) Palacios, M. A.; Nehrkorn, J.; Suturina, E. A.; Ruiz, E.; Gómez-Coca, S.; Holldack, K.; Schnegg, A.; Krzystek, J.; Moreno, J. M.; Colacio, E., Analysis of Magnetic Anisotropy and the Role of Magnetic Dilution in Triggering Single-Molecule Magnet (SMM) Behavior in

a Family of $Co^{II}Y^{III}$ Dinuclear Complexes with Easy-Plane Anisotropy. *Chem. -Eur. J.* **2017**, *23* (48), 11649-11661; (b) Colacio, E.; Ruiz, J.; Ruiz, E.; Cremades, E.; Krzystek, J.; Carretta, S.; Cano, J.; Guidi, T.; Wernsdorfer, W.; Brechin, E. K., Slow Magnetic Relaxation in a Co^{II}–Y^{III} Single-Ion Magnet with Positive Axial Zero-Field Splitting. *Angew. Chem. Int. Ed.* **2013**, *52* (35), 9130-9134.

8. (a) Shufang, X.; Yun-Nan, G.; Liviu, U.; Jinkui, T.; F., C. L., Tuning the Magnetic Interactions and Relaxation Dynamics of Dy_2 Single-Molecule Magnets. *Chem. -Eur. J.* **2015**, *21* (40), 14099-14106; (b) Apoorva, U.; Chinmoy, D.; Shefali, V.; Kumar, S. S.; Tulika, G.; Ranajit, M.; K., L. S.; S., M. K.; Gopalan, R.; Maheswaran, S., Role of the Diamagnetic Zinc(II) Ion in Determining the Electronic Structure of Lanthanide Single-Ion Magnets. *Chem. -Eur. J.* **2017**, *23* (20), 4903-4916; (c) Burrow, C. E.; Burchell, T. J.; Lin, P.-H.; Habib, F.; Wernsdorfer, W.; Clérac, R.; Murugesu, M., Salen-Based $[Zn_2Ln_3]$ Complexes with Fluorescence and Single-Molecule-Magnet Properties. *Inorg. Chem.* **2009**, *48* (17), 8051-8053; (d) Chakraborty, A.; Goura, J.; Kalita, P.; Swain, A.; Rajaraman, G.; Chandrasekhar, V., Heterometallic 3d–4f single molecule magnets containing diamagnetic metal ions. *Dalton Trans.* **2018**, *47* (27), 8841-8864; (e) Li, J.; Wei, R.-M.; Pu, T.-C.; Cao, F.; Yang, L.; Han, Y.; Zhang, Y.-Q.; Zuo, J.-L.; Song, Y., Tuning quantum tunnelling of magnetization through 3d–4f magnetic interactions: an alternative approach for manipulating single-molecule magnetism. *Inorg. Chem. Front.* **2017**, *4* (1), 114-122; (f) Oyarzabal, I.; Artetxe, B.; Rodríguez-Diéguez, A.; García, J. Á.; Seco, J. M.; Colacio, E., A family of acetato-diphenoxo triply bridged dimetallic $Zn^{II}Ln^{III}$ complexes: SMM behavior and luminescent properties. *Dalton Trans.* **2016**, *45* (23), 9712-9726; (g) Ruiz, J.; Lorusso, G.; Evangelisti, M.; Brechin, E. K.; Pope, S. J. A.; Colacio, E., Closely-Related $Zn^{II}_2Ln^{III}_2$ Complexes (Ln^{III} = Gd, Yb) with Either Magnetic Refrigerant or Luminescent Single-Molecule Magnet Properties. *Inorg. Chem.* **2014**, *53* (7), 3586-3594.

9. (a) Chandrasekhar, V.; Dey, A.; Mota, A. J.; Colacio, E., Slow Magnetic Relaxation in Co(III)–Co(II) Mixed-Valence Dinuclear Complexes with a $Co^{II}O_5X$ (X = Cl, Br, NO_3) Distorted-Octahedral Coordination Sphere. *Inorg. Chem.* **2013**, *52* (8), 4554-4561; (b) Zhu, Y.-Y.; Cui, C.; Zhang, Y.-Q.; Jia, J.-H.; Guo, X.; Gao, C.; Qian, K.; Jiang, S.-D.; Wang, B.-W.; Wang, Z.-M.; Gao, S., Zero-field slow magnetic relaxation from single Co(ii) ion: a transition metal single-molecule magnet with high anisotropy barrier. *Chem. Sci.* **2013**, *4* (4), 1802-1806.

10. Chakraborty, A.; Bag, P.; Rivière, E.; Mallah, T.; Chandrasekhar, V., Assembly of heterobimetallic Ni^{II}–Ln^{III} (Ln^{III} = Dy^{III}, Tb^{III}, Gd^{III}, Ho^{III}, Er^{III}, Y^{III}) complexes using a ferrocene ligand: slow relaxation of the magnetization in Dy^{III}, Tb^{III} and Ho^{III} analogues. *Dalton Trans.* **2014**, *43* (23), 8921-8932.

11. (a) Vogel, A. I.; Furniss, B. S.; Hannaford, A. J.; Smith, P. W. G.; Tatchell, A. R., *Vogel's textbook of practical organic chemistry. 5th ed*. Longman: Harlow, 1989; (b) Williams, D. B. G.; Lawton, M., Drying of Organic Solvents: Quantitative Evaluation of the Efficiency of Several Desiccants. *J. Org. Chem.* **2010**, *75* (24), 8351-8354.

12. Bruker Analytical X-ray Systems, I. M., WI, *SMART & SAINT Software Reference Manuals*, **2003**.

13. Sheldrick, G. M. *SADABS: A software for empirical absorption correction*, Ver. 2.05; University of Göttingen: Göttingen, Germany: **2002**.

14. *SHELXTL Reference Manual*, Bruker Analytical X-ray Systems, Inc.: Madison, WI: **2000**.

15. Sheldrick, G., A short history of SHELX. *Acta Crystallogr. A* **2008**, *64* (1), 112-122.

16. Dolomanov, O. V.; Bourhis, L. J.; Gildea, R. J.; Howard, J. A. K.; Puschmann, H., OLEX2: a complete structure solution, refinement and analysis program. *J. Appl. Crystallogr.* **2009**, *42* (2), 339-341.

17. Bradenburg, K. *Diamond, Ver. 3.1eM*, Crystal Impact GbR: Bonn, Germany,: **2005**.

18. (a) Neese, F., The ORCA program system. *Wiley Interdiscip. Rev. Comput. Mol. Sci.* **2012**, *2* (1), 73-78; (b) Aquilante, F.; Autschbach, J.; Carlson, R. K.; Chibotaru, L. F.; Delcey, M. G.; De Vico, L.; Fdez. Galván, I.; Ferré, N.; Frutos, L. M.; Gagliardi, L.; Garavelli, M.; Giussani, A.; Hoyer, C. E.; Li Manni, G.; Lischka, H.; Ma, D.; Malmqvist, P. Å.; Müller, T.; Nenov, A.; Olivucci, M.; Pedersen, T. B.; Peng, D.; Plasser, F.; Pritchard, B.; Reiher, M.; Rivalta, I.; Schapiro, I.; Segarra-Martí, J.; Stenrup, M.; Truhlar, D. G.; Ungur, L.; Valentini, A.; Vancoillie, S.; Veryazov, V.; Vysotskiy, V. P.; Weingart, O.; Zapata, F.; Lindh, R., Molcas 8: New capabilities for multiconfigurational quantum chemical calculations across the periodic table. *J. Comput. Chem.* **2016**, *37* (5), 506-541; (c) Aquilante, F.; De Vico, L.; Ferré, N.; Ghigo, G.; Malmqvist, P.-å.; Neogrády, P.; Pedersen, T. B.; Pitoňák, M.; Reiher, M.; Roos, B. O.; Serrano-Andrés, L.; Urban, M.; Veryazov, V.; Lindh, R., MOLCAS 7: The Next Generation. *J. Comput. Chem.* **2010**, *31* (1), 224-247; (d) Chibotaru, L. F.; Ungur, L., *Ab initio* calculation of anisotropic magnetic properties of complexes. I. Unique definition of pseudospin Hamiltonians and their derivation. *J. Chem. Phys.* **2012**, *137* (6), 064112.

19. (a) Weigend, F.; Ahlrichs, R., Balanced basis sets of split valence, triple zeta valence and quadruple zeta valence quality for H to Rn: Design and assessment of accuracy. *Phys. Chem. Chem. Phys.* **2005**, *7* (18), 3297-3305; (b) Maurice, R.; Bastardis, R.; Graaf, C. d.; Suaud, N.; Mallah, T.; Guihéry, N., Universal Theoretical Approach to Extract Anisotropic Spin Hamiltonians. *J. Chem. Theory Comput.* **2009**, *5* (11), 2977-2984.

20. Roos, B. O.; Lindh, R.; Malmqvist, P.-Å.; Veryazov, V.; Widmark, P.-O.; Borin, A. C., New Relativistic Atomic Natural Orbital Basis Sets for Lanthanide Atoms with Applications to the Ce Diatom and LuF_3. *J. Phys. Chem. A* **2008**, *112* (45), 11431-11435.

21. (a) Rouvray, D. H.; Hargittai, I., Concepts in Chemistry - A Contemporary Challenge. *Angew. Chem. Int. Ed.* **1997**, *36* (22), 2525; (b) Zabrodsky, H.; Peleg, S.; Avnir, D., Continuous symmetry measures. *J. Am. Chem. Soc.* **1992**, *114* (20), 7843-7851.

22. Kahn, O., *Molecular Magnetism*. VCH Publishers, New York: **1993**.

23. Dekker, C.; Arts, A. F. M.; de Wijn, H. W.; van Duyneveldt, A. J.; Mydosh, J. A., Activated dynamics in a two-dimensional Ising spin glass: $Rb_2Cu_{1-x}Co_xF_4$. *Phys. Rev. B* **1989**, *40* (16), 11243-11251.

24. Cole, K. S.; Cole, R. H., Dispersion and Absorption in Dielectrics I. Alternating Current Characteristics. *J. Chem. Phys.* **1941**, *9* (4), 341-351.

25. Eichhöfer, A.; Lan, Y.; Mereacre, V.; Bodenstein, T.; Weigend, F., Slow Magnetic Relaxation in Trigonal-Planar Mononuclear Fe(II) and Co(II) Bis(trimethylsilyl)amido Complexes—A Comparative Study. *Inorg. Chem.* **2014**, *53* (4), 1962-1974.

26. Gomez-Coca, S.; Cremades, E.; Aliaga-Alcalde, N.; Ruiz, E., Mononuclear Single-Molecule Magnets: Tailoring the Magnetic Anisotropy of First-Row Transition-Metal Complexes. *J. Am. Chem. Soc.* **2013**, *135* (18), 7010-7018.

27. Chattopadhyay, K.; Heras Ojea, M. J.; Sarkar, A.; Murrie, M.; Rajaraman, G.; Ray, D., Trapping of a Pseudotetrahedral $Co^{II}O_4$ Core in Mixed-Valence Mixed-Geometry $[Co_5]$ Coordination Aggregates: Synthetic Marvel, Structures, and Magnetism. *Inorg. Chem.* **2018**, *57* (21), 13176-13187.

"For Table of Contents Use Only"

Slow Magnetic Relaxation in Dinuclear $Co^{II}Y^{III}$ Complexes

*Joydev Acharya,[a] Abinash Swain,[b] Amit Chakraborty,[a,d] Vierandra Kumar,[a] Pawan Kumar,[a] Jessica Flores Gonzalez,[c] Olivier Cador,[c] Fabrice Pointillart,[*c] Gopalan Rajaraman,[*b] and Vadapalli Chandrasekhar[*a,d]*

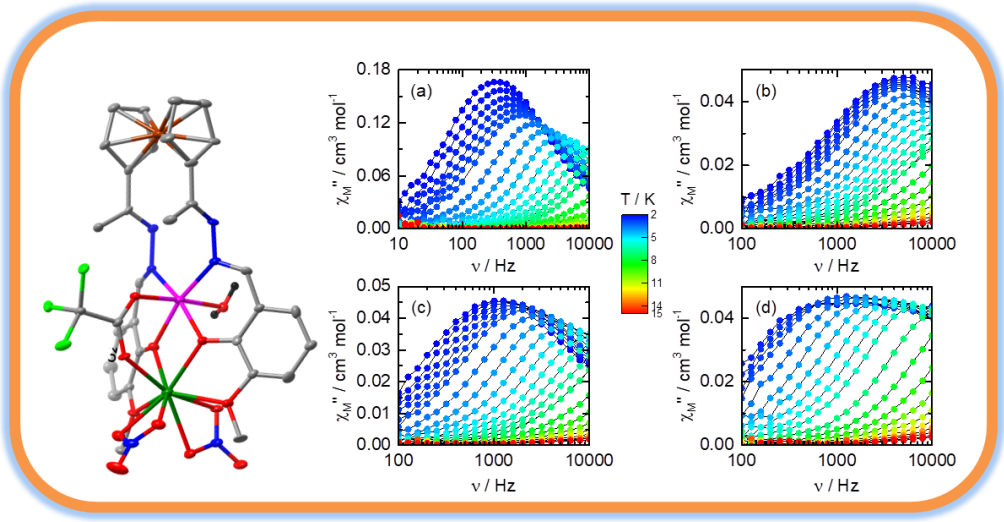

Four iso-structural molecules having common $Co^{II}Y^{III}$ core have been synthesized where the bridging acetate groups between Co^{II} and Y^{III} are altered. The effect of substitution on bridging ligands on magnetic properties of the molecules has been estimated by combined experimental and theoretical studies.